JMEPEG (2012) 21:2643–2649
DOI: 10.1007/s11665-012-0390-1

1059-9495/$19.00

Continuous Rotary Motor Actuated by Multiple Segments of Shape Memory Alloy Wires

X.Y. Zhang and X.J. Yan

(Submitted February 16, 2012; in revised form May 19, 2012)

An attempt has been made in this study to develop a continuous rotary motor actuated by multiple segments of shape memory alloy wires (SMA motor). In order to meet the requirements of continuous rotation, large output torque, and stall torque, a unidirectional rotary actuator was designed, and five rotary actuators were fixed on one shaft in series. When every actuator is actuated in turn, the SMA motor can realize a continuous rotation. In order to simulate the rotation angle, output torque, and the actuation performance degradation of the SMA motor, Lagoudas's constitutive model was modified to consider the cyclic actuation influence. After design and simulation, a prototype of the SMA motor was fabricated and experimentally tested to verify the feasibility and performance of the proposed design decision. The test results indicate that the SMA motor can realize continuous rotation. The rotation speed is 0.28 r/min, and the torque is 1008 N mm.

Keywords actuator, performance degradation, shape memory alloy, SMA rotary motor

1. Introduction

This article describes an attempt that has been made to develop a continuous rotation motor actuated by multiple segments of shape memory alloy wires (SMA motor). The currently used electrical motors, which are based on electromagnetic induction principle, are very useful to drive systems working with high rotation speed. However, for some applications very slow actuation is needed, such as the deployment of solar arrays on the satellite and the robotic arms, the lifelike robotic muscles. The conventional motor in such applications requires large gear reduction, which makes the actuator system bulky and uneconomic. Therefore, a motor which can ideally generate a large torque and rotate slowly is urgently needed.

Shape memory alloy (SMA) possesses an ability to remember its original shape and revert to it at a characteristic transformation temperature. It also has unparalleled energy and power density (up to 30 MJ m^{-3} and 700 kW m^{-3}), and significantly large operating stresses and strains (up to 200 MPa and 4.5% strain), and maximum stress and strain for low cycle applications (up to 700 MPa and 8% strain) (Ref 1). These advantages make SMA very suitable for simpler, lighter, more compact, and larger driving force actuators.

SMA has been utilized to develop rotary actuators by some researchers because of its remarkable performance. Tanaka and Yamada (Ref 2) designed a rotary actuator using two segments of 0.3-mm-diameter SMA wires. However, the actuator can only provide limited rotational actuation. Another rotary actuator described by Weimin Huang consists of a SMA wire, a macor disk, and a steel shaft (Ref 3). The SMA wire is wound on the macor disk. One end of the wire is fixed to the macor disk, while the other end is fixed to the base plate. The SMA wire shrinks, and the macor disk rotates to the extent of wire shrinkage after heating. Similar to Tanaka and Yamada's actuator, the latter actuator can only provide limited rotational actuation, and the maximum rotation angle is 120°. Carpenter and others (Ref 4) presented a rotary actuator using SMA helical spring. In their design scheme, NiTiCu alloy wires have been wound into helical spring actuators to control the gimbal rotation using mechanical elements to convert the linear motion of antagonistic SMA springs into rotation. The gimbal can rotate from −100° to +100° at a rotation rate of 0.06°/s, and has a maximum output torque of 0.34 N m. Reference 5 also reported rotary manipulators using SMA wire-actuated flexures. The aforementioned rotary SMA actuators cannot provide continuous rotary output. To overcome this drawback, some researchers attempted to develop continuous rotary SMA actuator (namely SMA motor).

Kuribayashi (Ref 6) reported an attempt to develop a servomotor. The motor uses compressive SMA strips as springs in bending mode, and can rotate continuously. However, Ref 7 showed that the strips have less energy density than SMA wires. Correspondingly, the servomotor has less energy density. Sharma et al. (Ref 8) realized the drawback and designed a SMA wire-based poly phase rotary motor. The motor, which is composed of three phases, uses SMA wire of diameter 0.35 mm and of length 120 mm with a tension spring in series for each phase of the motor. The motor can rotate with a rotational speed of 0.125 r/s, and the output torque is 2 kg mm. However, as the three phases are fixed to one cam, when one of the phases is actuated to drive the cam, it has to stretch the remaining two

This article is an invited paper selected from presentations at the International Conference on Shape Memory and Superelastic Technologies 2011, held November 6-9, 2011, in Hong Kong, China, and has been expanded from the original presentation.

X.Y. Zhang and **X.J. Yan**, Group405, School of Jet Propulsion, BeiHang University, Beijing, China. Contact e-mail: zhangyong 9119@163.com.

phases, which will greatly decrease the net driving force. Thus, the poly phase rotary motor has a fairly small output torque. Hideki Okamura designed a light-driven SMA motor which is operated by a single source of light (Ref 9). The device utilizes a NiTi SMA wire initially trained to straight shape. The SMA wire is formed in a loop and put around two wheels. When the SMA wire is heated by a light, it shrinks to rotate the wheel by a friction force between the SMA wire and the wheel. Experimental results showed that the motor can achieve a steady and continuous rotation with a bundled loop of 0.3-mm-diameter wire. Unfortunately, as the wheel was rotated by the frictional force between the SMA wire and the wheel, the output torque is limited.

Moreover, the reported SMA wire-based motors all have a limited stall torque, which means when the load to be actuated is larger than the stall torque, the motors may rotate in the opposite direction. However, for some applications, the counter rotation of the motors is very dangerous, and so a comparative larger stall torque is needed.

Reference 10 showed that the actuation performance degradation of SMA due to cyclic actuation is very significant. This factor must be considered while designing the SMA-based actuator, especially when the actuator needs to work for many times. When SMA wires are used to develop motors, they will undergo tens of thousands of actuation during their service life, and hence the cyclic actuation degradation must be considered.

The objective of this article was to design and fabricate a novel rotary SMA wire-actuated motor which possesses the ability of continuous rotation, large torque output, and large stall torque. To simulate the performance, degradation of the SMA motor was considered, and a modified SMA constitutive model which can describe the degradation of SMA wire due to cyclic actuation was derived.

The layout of the article is as follows: In the second section, the conceptual design of the SMA motor is presented and the working principle is explained. In the third section, the rotary actuator is designed, and the performances of the actuator are simulated. Experimental verifications are carried out in the fourth section. The present study is then summarized in the fifth section.

2. Conceptual Design and Working Principle

The SMA motor to be developed in this investigation should possess the ability of continuous rotation, large output torque, and large stall torque. This section describes the conceptual design and working principle of the SMA motor.

The SMA wire usually generates a linear movement, and so the first step to design a rotary SMA wire-based motor is to translate the linear movement produced by the SMA wire into rotary motion of the motor shaft. For this purpose, a rotary actuator must be first designed.

The rotary actuator is the most important component of the motor; the actuation performance of the actuator can significantly influence the output characteristic of the motor. The purpose of this study is to develop a SMA motor which has a large output torque and stall torque, and therefore the rotary actuator must also possess the same abilities.

As mentioned in the first section, the SMA wire-based motors described in Ref 8 and Ref 9 have the drawback of small output torque. For the poly phase rotary motor (Ref 8), the three actuation phases are mechanically fixed to the same cam; while one of the phases acts as a driving source, the remaining two phases act as resistance sources. For the light-driven SMA motor (Ref 9), the frictional force between the SMA wire and the wheel is used to drive the wheel. To design a large output torque rotary actuator, two issues must be taken into account: (1) a "rigid" motion pair required to transform the SMA wire's linear movement into rotary motion, and (2) every rotary actuator (like the phrase in Ref 8) "can work freely."

Considering the first issue, we proposed a rotary actuator design decision, as shown in Fig. 1. The rotary actuator is composed of six parts: 1 SMA wire, 2 friction pawl, 3 friction ratchet wheel, 4 brake pawl, 5 bias spring, and 6 shaft. The ratchet-pawl mechanism is used to transform the SMA wire's linear movement into rotary motion. Ratchet-pawl mechanism is a kind of "rigid" motion pair, and hence, it can completely transform the driving force generated by SMA wire into output torque of the shaft. In addition, because of the brake pawl, the friction ratchet wheel can only rotate anticlockwise, which means that the stall torque of the rotary actuator is infinite.

Based on the current design concept, the SMA wire rotary actuator was physically implemented, as shown in Fig. 2. As long lengths of SMA wire were required to produce ample displacement, a pulley architecture was implemented to package the SMA wire to realize a compact dimension. To adjust the preload produced by the bias spring after the SMA wire is fixed, we designed an adjusting nut, as shown in Fig. 2.

The rotary actuator can only generate a unidirectional, intermittent rotation; however, what we really need is continuous rotation output. To realize it, five rotary actuators are fixed in a series on a shaft, as shown in Fig. 3. When these rotary actuators are actuated in turn, the shaft can rotate continuously.

The second issue requires every rotary actuator to work freely to gain a larger output torque. As shown in Fig. 1, when the SMA wire is heated by an electric current, it will shrink to rotate the friction ratchet wheel through the friction pawl to produce an output torque. During the heating process, the ratchet wheel in Fig. 1 (named drive wheel) will rotate, and drive all the remaining wheels (named idler wheels) to rotate. And fortunately, all the idler wheels can rotate freely, without being blocked by any pawl, because the working principle of

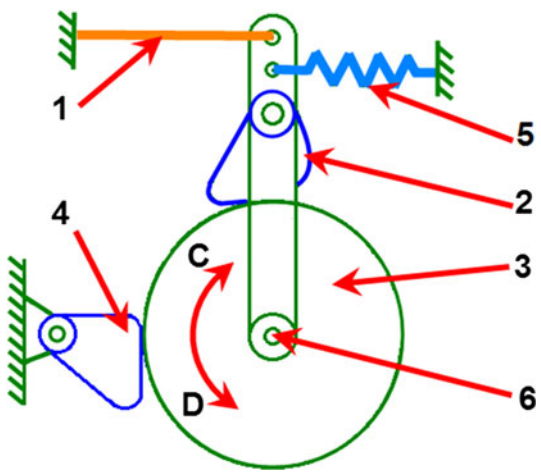

Fig. 1 Concept of SMA wire-based rotary actuator. 1, SMA wire; 2, friction pawl; 3, friction ratchet wheel; 4, brake pawl; 5, bias spring; and 6, shaft

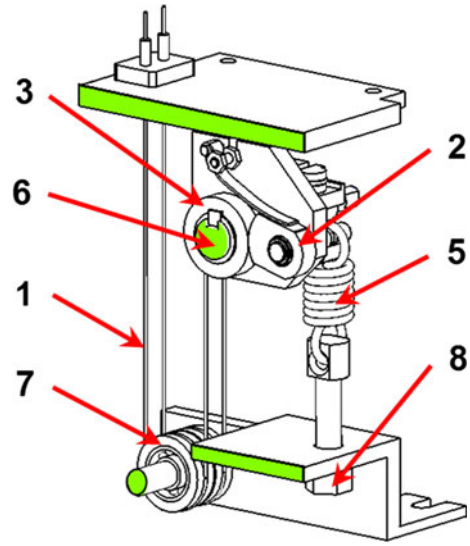

Fig. 2 Implementation of the SMA wire-based rotary actuator. 1, SMA wire; 2, friction pawl; 3, friction ratchet wheel; 5 bias spring; 6, shaft; 7, pulleys; and 8 adjusting nut

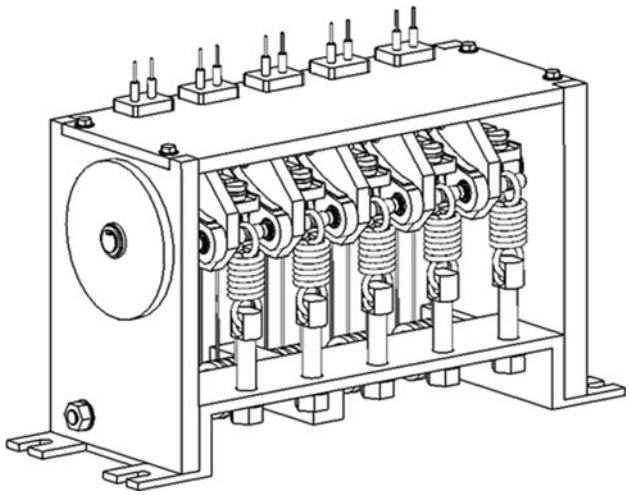

Fig. 3 General architecture of the SMA motor

ratchet-pawl mechanism prevents the ratchet wheel from driving the pawl.

With the design of the rotary actuator and the general architecture of the SMA motor being completed as above, the motor finally meets the requirements of large output torque, large stall torque, and continuous rotation. In the next section, the design and simulation of the rotary actuator will be presented.

3. Design and Simulations of the SMA Motor

The rotary actuator illustrated in Fig. 1 is simply composed of a SMA wire, a bias spring, and a ratchet-pawl mechanism. It can be described by a simple model as shown in Fig. 4. The objectives of actuator design and simulation are to find a proper

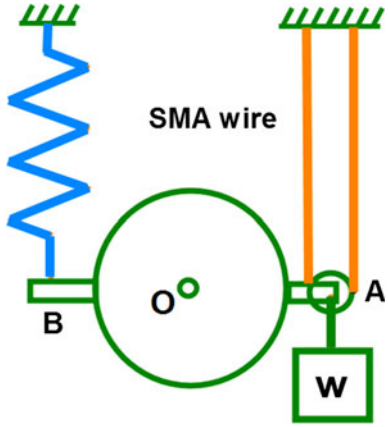

Fig. 4 A simplified model of the rotary actuator

bias spring to work with SMA wire and simulate the output performances of the rotary actuator and the SMA motor.

3.1 Design Principle and Method

As shown in Fig. 4, the motion of the ratchet wheel depends on the force relationship between the SMA wire, bias spring, and the load W: When the SMA wire is heated, the recovery force generated by the SMA wire is larger than the force provided by the bias spring plus the load W. Therefore, the bias spring is stretched. Meanwhile, the ratchet wheel rotates anticlockwise; when the current supply is cut off, the SMA wire becomes cold, and the recovery force disappears. However, the forces provided by the bias spring and the load W still exist, and so the bias spring rotates the ratchet wheel clockwise and stretches the SMA wire to its original length.

During the whole actuation process, the position of the ratchet wheel is controlled by five variables of forces: $F_{\min}$, $F_{\max}$, F_r, F_f, and W, where $F_{\min}$ and $F_{\max}$ are, respectively, the minimum and maximum forces provided by bias spring; F_r is the recovery force generated by SMA wire when heated; F_f is the yield force of SMA wire after cooling down; and W is the required output force of the rotary actuator. F_f and F_r can be easily obtained through uniaxial tensile and recovery tests of SMA wire; W is determined by the required output torque of the rotary actuator; $F_{\min}$ must be larger than F_f to insure that the bias spring can draw the SMA wire to its initial length after heating, and so the value of $F_{\min}$ depends on F_f; the sum of $F_{\max}$ and W must be smaller than F_r to insure that the SMA wire can stretch the bias spring and rotate the ratchet wheel, and so the value of $F_{\max}$ depends on W and F_r. Based on the above analysis, the relationship between $F_{\min}$ and F_b can be expressed as

$$F_{\min} + W \geq F_f. \quad \text{(Eq 1)}$$

and the relationship between $F_{\max}$, W, and F_r can be represented as

$$F_{\max} + W \leq F_r. \quad \text{(Eq 2)}$$

If the SMA wire can generate a recovery strain ε_r after heating, then the stiffness of the bias spring is given by

$$k = (F_{\max} - F_{\min})/L\varepsilon_r. \quad \text{(Eq 3)}$$

where L is the original length of the SMA wire, and k is the stiffness of the bias spring.

In order to design a proper bias spring, F_{max}, F_{min}, and k must be given as prior parameters. From Eq 1-3, it is obvious that the three parameters are dependent on F_f, F_r, L, and ε_r, where L is the original length of SMA wire, which can be determined during structure design; F_f and F_r depend on the corresponding stresses σ_f and σ_r, which can be obtained through experiments. Also, the recovery strain ε_r can be determined from experiments.

Using the design principle and the method described above, the parameters of the rotary actuator were calculated, which are listed in Table 1.

3.2 Material Model

The rotary actuator design has been done, and the design results will be used to simulate the performance of the rotary actuator in this section. A material model should be chosen to characterize the behavior of the SMA wire. Several numerical approaches have been presented in respect of modeling the properties and the behavior of SMA in the literature. For example, Liang and Rogers (Ref 11) and Qidwai and Lagoudas (Ref 12) have developed thermodynamic models for SMA. The constitutive model developed by Lagoudas will be adopted in this article. This model has been validated and provides a description of the SMA uniaxial stress and strain behavior, which is well suited to the actuator element considered here. Detailed discussion about the constitutive model is found in Ref 12.

As mentioned above, the performance degradation of the SMA wire must be considered in the actuator simulation. Unfortunately, Lagoudas's constitutive model cannot describe this behavior, and so we made some modifications to the model.

First of all, the accumulated martensite volume fraction was defined, and the expression is given as

$$\xi^{c} = \xi^{ac} + \xi^{mc}, \qquad \text{(Eq 4)}$$

where

$$\xi^{ac} = \int \left|\dot{\xi}^{a\to m}\right| dt \quad \xi^{mc} = \int \left|\dot{\xi}^{m\to a}\right| dt. \qquad \text{(Eq 5)}$$

where, ξ^{ac} denotes the accumulated martensite volume fraction during the transformation from austenite to martensite; ξ^{mc} denotes the accumulated martensite volume fraction during the reverse transformation.

The evolution of the transformation-induced plastic strain is expressed as

$$\varepsilon^{p} = \varepsilon^{p}_{max} e^{-\xi_c m}, \qquad \text{(Eq 6)}$$

where ε^{p}_{max} is the maximum plastic strain produced during cyclic actuations.

The evolution of the maximum uniaxial transformation strain is expressed as

Table 1 SMA wire-based rotary actuator parameters

Parameters	Value
Bias spring stiffness, N/mm	25
Length of wires, mm	105
Diameter of SMA wires, mm	0.5
Actuation distance, mm	3.8
Output force, N	63

$$H'(\xi_c) = H_0 + H_{max}\left(1 - e^{-\xi_c n}\right) \qquad \text{(Eq 7)}$$

where, H_0 is the initial maximum uniaxial transformation strain, and H_{max} is the growth of the maximum uniaxial transformation strain during cyclic actuation.

With the expression (7), the flow law of the transformation strain becomes as follows:

$$\dot{\varepsilon}^{t} = \dot{\xi}^{d} H' \qquad \text{(Eq 8)}$$

Finally, the total strain can be expressed as

$$\varepsilon = \varepsilon^{t} + \varepsilon^{p} + \varepsilon^{e} \qquad \text{(Eq 9)}$$

where, m and n are the parameters controlling the evolutions of the transformation-induced plastic strain and the maximum uniaxial transformation strain, respectively.

3.3 Simulation of the Rotary Actuator and SMA Motor

Based on the material parameters obtained from the experimental results in the monotonic tension or compression and certain cyclic actuation tests, and using the actuator parameters in Table 1, the output torque and angle of a single rotary actuator were simulated, and the results are shown in Fig. 5 and 6. It is seen from the figures that (1) the maximum output torque of the rotary actuator is 1008 N mm; and (2) The maximum output angle is 14.5°.

The output performances of the SMA motor were then simulated using the modified constitutive model. The output torque and angle of the SMA motor are shown in Fig. 7 and 8, respectively. It can be concluded from these figures that (1) the output torque is not constant, and it assumes waveform as the rotary actuators work in turn; and (2) The rotation angle of the SMA motor increases monotonously as the rotary actuators work in turn, and the rotational speed is about 0.52 r/min.

As mentioned above, the actuation performance degradation of the rotary actuator must be considered. The degradation behavior was studied using the modified constitutive model, and the simulation results are shown in Fig. 9 and 10. It is seen from the results that (1) the strain-temperature loop keeps shrinking and moving up, which implies that the plastic strain is accumulating and the recovery strain is decreasing with the increasing actuation times. (2) The pure recovery strain drops from 4.05 to 3.65%, and finally remains stable.

4. Proof-of-Concept Experiments and Discussion

A prototype of the SMA motor was fabricated and experimentally tested to verify the feasibility and performance of the proposed design decision. The envelope of the prototype (shown in Fig. 11) is $140 \times 90 \times 60$ mm^3, and the experimental setup for the rotation angle test is shown in Fig. 12.

4.1 Testing Experiments

The rotation angle of a single rotary actuator was tested using the setup shown in Fig. 12. The test result was compared with the simulated one, as shown in Fig. 6. It can be seen from the figure that the experimental data show a good agreement with the simulation data, and that the maximum rotation angle is 14.5°.

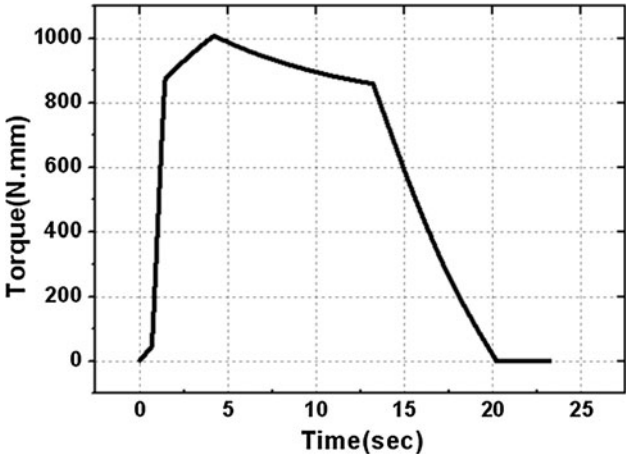

Fig. 5 Output torque of the rotary actuator

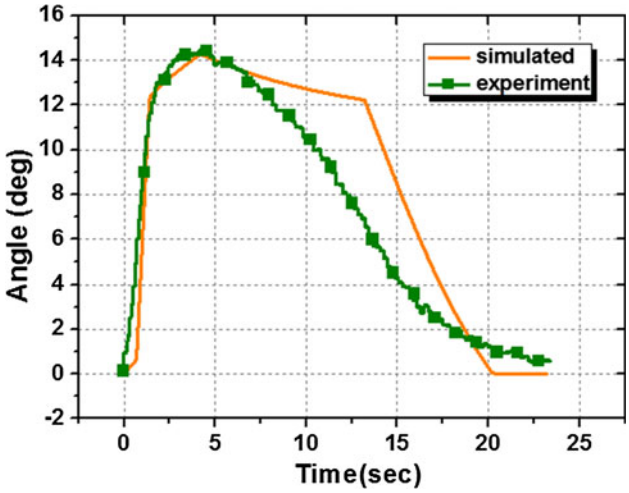

Fig. 6 Output angle of the rotary actuator (simulation vs. experiment)

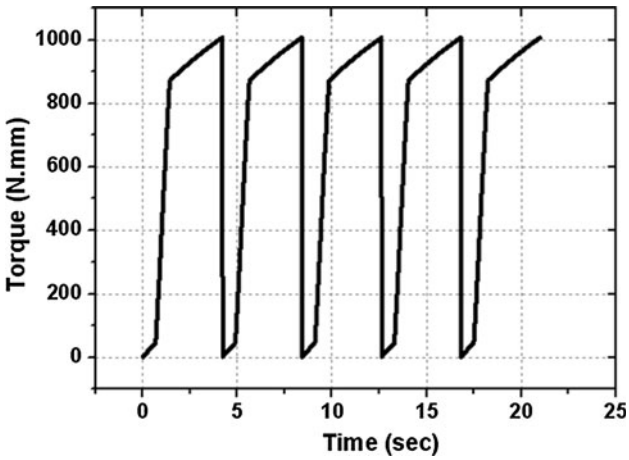

Fig. 7 Output torque of the SMA motor

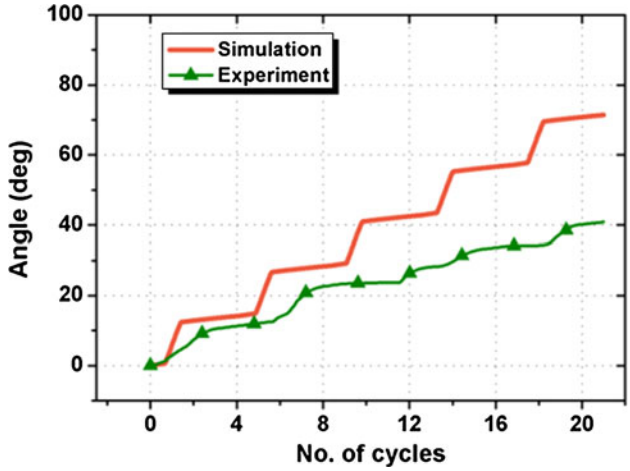

Fig. 8 Output angle of the SMA motor (simulation vs. experiment)

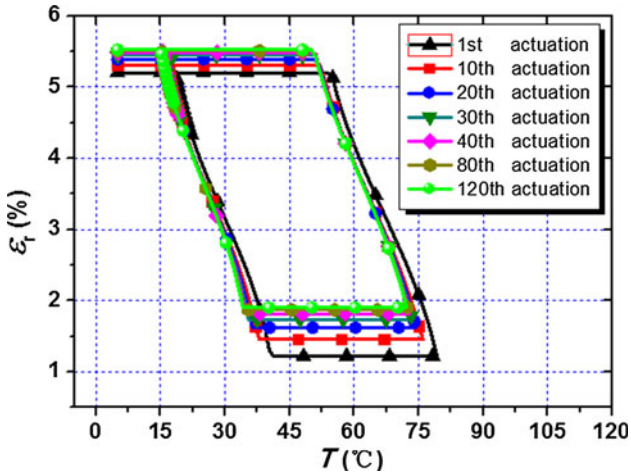

Fig. 9 Strain-temperature curve of cyclic actuation of the rotary actuator

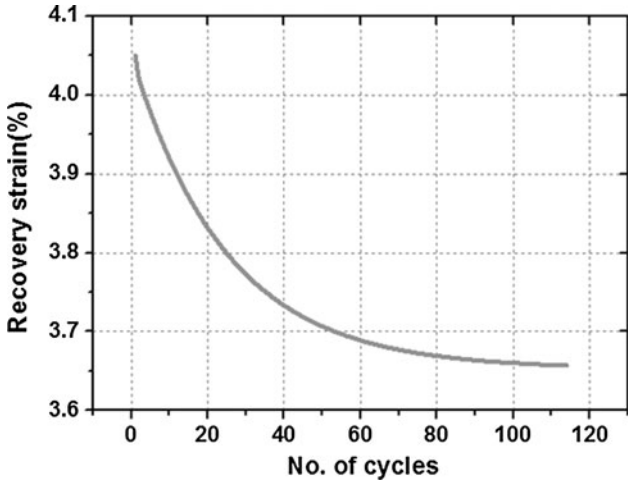

Fig. 10 Recovery strain curve of cyclic actuation of the rotary actuator

The rotation angle of the SMA motor was also tested, and the test results were compared with the simulated one, as shown in Fig. 8. From the figure, it is observed that the test results are very different from the simulated ones. The rotational speed determined from the test results is 0.28 r/min, whereas the speed determined from the simulation results is 0.52 r/min.

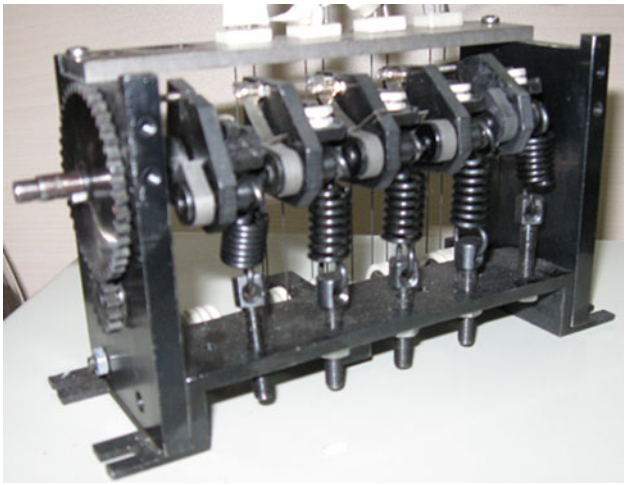

Fig. 11 Prototype of the SMA motor

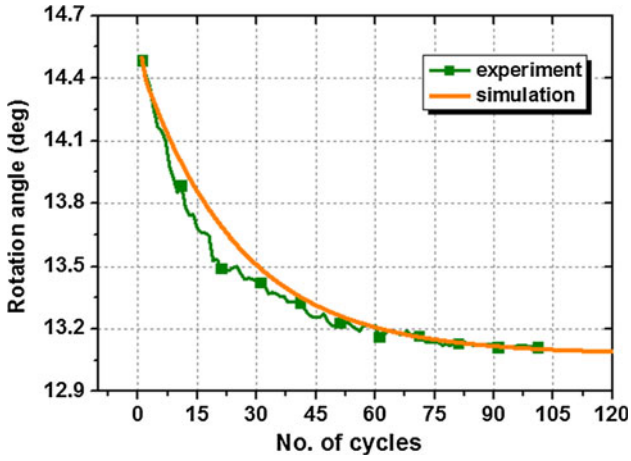

Fig. 13 The degradation of output angle of the rotary actuator (simulation vs. experiment)

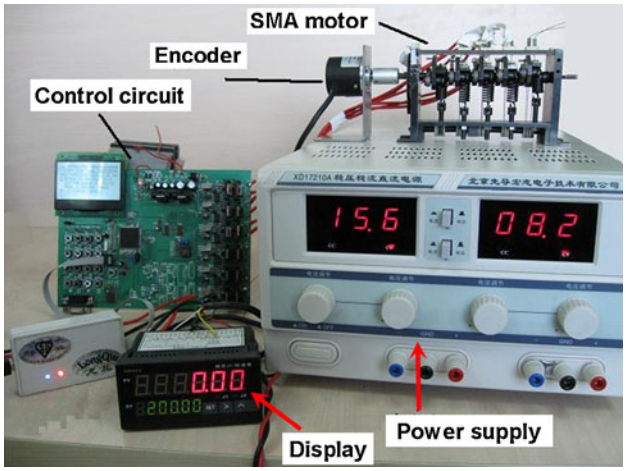

Fig. 12 Experiment setup for the rotation angle test

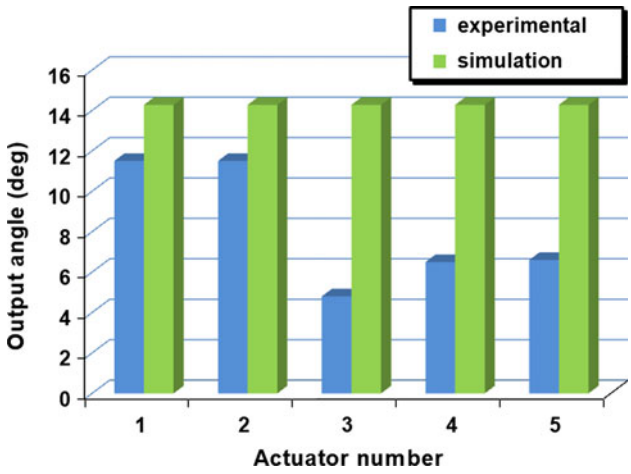

Fig. 14 Output displacement of individual actuator (experimental vs. simulation)

Output angles of the rotary actuator for 100 actuation times were tested, and the test results show a good agreement with the simulated results, as shown in Fig. 13. From the figure, it can be seen that the output angle decreases from 14.5° to 13.6°, and finally remains stable at 13.6°.

5. Discussion

We found that the test results of the SMA motor rotation angle are very different from the simulated ones, as shown in Fig. 8. We observed the whole working process of the SMA motor and found that the friction pawl slid on the friction wheel before they are geared into each other, which decreases the output angle of the SMA motor.

In addition, the actual measured rotation angles for individual actuators vary greatly, and as shown in Fig. 14, they vary from 4.8° to 11.5°. We investigated into the actuation process of every individual actuator and found that the causes of the output deviations are most likely due to tolerance errors from the manufacturing and assembly, especially from the friction pawl and the ratchet wheel. The actual distance between the hinge center of the friction pawl and the center of the ratchet wheel, as shown in Fig. 15, is different for every actuator. For the actuator with large tolerance error, more output displacement produced by the SMA wire will be wasted in gearing the friction pawl into the ratchet wheel, which results in a smaller output angle; however, for the actuator with smaller tolerance error, less output distance will be wasted, and thus a larger output angle can be achieved.

As shown in Fig. 8, the torque profile consists of serious ripples, which may limit the application of the rotary motor. However, these torque ripples can be reduced via the improvement of the control strategy. The currently applied strategy only allows to power the following actuator after cutting off the power to the former one. At the power shifting moment, the output torque will reasonably decrease, and a torque ripple arises. If the strategy allows to power the following one before cutting off the power to the former one, the output torque will become more stable. This article emphasizes on the mechanism aspect of the SMA motor. Some remarkable studies referring to control strategies of SMA wire-based actuators have been done (Ref 13, 14). Based on these studies, more experiments will be

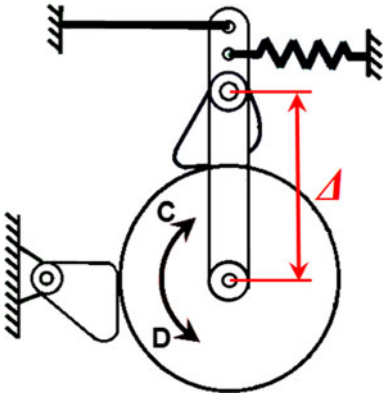

Fig. 15 The distance between the friction pawl and the ratchet wheel

needed, focusing on the control strategy optimization in a future study.

6. Summary and Conclusion

In this study, a novel prototype of a continuous rotary SMA motor with the advantages of larger output torque and stall torque was designed and fabricated. In order to simulate the output degradation of the SMA motor, Lagoudas's constitutive model was modified, and the modified model was used to simulate the output performance of the SMA motor. After design and simulation, a prototype of the SMA motor was fabricated and experimentally tested to verify the feasibility and performance of the proposed design decision. The test results show that the SMA motor can realize continuous rotation. The rotation speed is 0.28 r/min, and the torque is 1008 N mm.

Future study will set emphasis on the following issues:

1. For the currently proposed design, the friction pawl tends to slide on the ratchet wheel. Hence, an improvement should be made to the friction pawl and ratchet wheel mechanism in the future study.
2. Tolerance errors from the manufacturing and assembly should be taken into account.
3. An optimized control strategy will be developed to reduce the output torque ripples.
4. Current cyclic degradation tests for the SMA actuator only last for 100 times, which are not sufficient for the SMA motor application. Future studies will focus on cyclic degradation tests for more actuation cycles.

Acknowledgments

This study was supported by the Foundation for the Author of National Natural Science Foundation of China (NSFC, Approved No. 10872015).

References

1. D.J. Hartl and D.C. Lagoudas, Aerospace Applications of Shape Memory Alloys, *Proc. IMechE G*, 2007, **221**, p 535–552
2. Y. Tanaka and A. Yamada, A Rotary Actuator Using Shape Memory Alloy for a Robot-Analysis of the Response With Load, *Proceedings IROS'91. IEEE/RSJ International Workshop on Intelligent Robots and Systems'91. Intelligence for Mechanical Systems, IEEE*, 1991, vol 2, p 1163–1168
3. W. Huang, Shape Memory Alloys and Their Application to Actuators for Deployable Structures, *Dissertation Submitted to the University of Cambridge for the Degree of Doctor of Philosophy*, 1998, p 116–121
4. B.F. Carpenter, R.J. Head, and R. Gehling, Shape Memory Actuated Gimbal, *Proc. SPIE*, 1995, **2447**, p 90–101
5. C.C. Lan, J.H. Wang, and C.H. Fan, Physical Optimal Design of Rotary Manipulators Using Shape Memory Alloy Wire Actuated Flexures, *Sens. Actuators A*, 2009, **153**, p 258–266
6. K. Kuribayashi, A New Servomotor Using Shape Memory Alloy, *IECON'89. 15th Annual Conference of IEEE, Industrial Electronics Society*, November 1989, vol 1, p 238–243
7. M.A. Warith, K. Kennedy, R. Reitsma, D. Reynaerts, and H.V. Brussel, Design Aspects of Shape Memory Actuators, *Mechatronics*, 1998, **8**(6), p 635–656
8. S.V. Sharma, M.M. Nayak, and N.S. Dinesh, Modelling, Design and Characterization of Shape Memory Alloy-Based Poly Phase Motor, *Sens. Actuators A*, 2008, **147**, p 583–592
9. H. Okamura, Light-Driven Motor, *Opt. Eng.*, 2011, **50**(2), p 71–73
10. N.G. Jones and D. Dye, Martensite Evolution in a NiTi Shape Memory Alloy when Thermal Cycling Under an Applied Load, *Intermetallics*, 2011, **19**(10), p 1348–1358
11. C. Liang and C.A. Rogers, One-Dimensional Thermo-Mechanical Constitutive Relations for Shape Memory Materials, *J. Intell. Mater. Syst. Struct.*, 1990, **1**(4), p 207–234
12. M.A. Qidwai and D.C. Lagoudas, Numerical Implementation of a Shape Memory Alloy Thermomechanical Constitutive Model Using Return Mapping Algorithms, *Int. J. Numer. Methods Eng.*, 2000, **47**(9), p 1123–1168
13. Y.H. Teh and R. Featherstone, An Architecture for Fast and Accurate Control of Shape Memory Alloy Actuators, *Int. J. Robot. Res.*, 2008, **27**(5), p 595–611
14. G. Song, Design and Control of a Nitinol Wire Actuated Rotary Servo, *Smart Mater. Struct.*, 2007, **16**, p 1796–1801